Acta Oceanol. Sin., 2025, Vol. 44, No. 2, P. 104–113
https://doi.org/10.1007/s13131-024-2398-4

Time bias compensation model considering multi-layer sound speed perturbation for underwater acoustic positioning

Yuanxi Yang[1, 2], Shengqiu Zhang[3*], Shuqiang Xue[4]

[1] State Key Laboratory of Spatial Datum, Xi'an 710054, China
[2] Xi'an Research Institute of Surveying and Mapping, Xi'an 710054, China
[3] School of Geological and Surveying Engineering, Chang'an University, Xi'an 710054, China
[4] Chinese Academy of Surveying and Mapping, Beijing 100036, China

Received 9 July 2024; accepted 1 November 2024

Abstract
Spatio-temporal variation of sound speed, in seafloor geodetic precise positioning, can always be attributed to the time error. Firstly, this paper analyzes the existing error compensation model, i.e., the time ratio model, which is expressed by the recorded time multiplying a ratio coefficient. And then a time split model is proposed by expressing the acoustic ray traveling time as the recorded time pluses a perturbation time error. The theoretical differences between the proposed time bias compensation model and the time ratio model are analyzed. Under the new framework, sound speed perturbation models with optimal single-layer spatial gradient and multi-layer spatial gradients are developed to compensate for sound speed error in the complex cases. Numerical computation shows that the simple time split model keeps the same accuracy as some complicated models while considering the distribution of random error. Furthermore, multi-layer model can improve the positioning accuracy without putting the pressure on parametrization.

Key words seafloor geodesy, underwater positioning, GNSS-acoustic, sound speed error, resilient observation model

Citation Yang Yuanxi, Zhang Shengqiu, Xue Shuqiang. 2025. Time bias compensation model considering multi-layer sound speed perturbation for underwater acoustic positioning. Acta Oceanologica Sinica, 44(2): 104–113, doi: 10.1007/s13131-024-2398-4

1 Introduction

Global Navigation Satellite System-Acoustic (GNSS-A) is the most useful technique for submarine positioning and navigation (Yang et al., 2020). The precise point positioning (PPP)-Acoustic (PPP-A) is much more helpful for the ocean real-time positioning, especially the satellite-based PPP provided by BeiDou global navigation satellite system (BDS-3), because it broadcasts the precise satellite orbit and clock correction by the Geostationary (GEO) satellites, rather than the Internet (Li et al., 2022; Yang et al., 2022; Zhang and Wang, 2023). The key issue of the GNSS-A underwater positioning is the acoustic observation model error compensation, in which the sound speed variation in different environments should be carefully taken into account (Chen et al., 2019; Qin et al., 2022, 2023; Yang and Qin, 2021; Zhao et al., 2021). As we know that the sound speed is different in different region, even at different depth or different direction at the same region due to the inhomogeneity of the water column density (Yamada et al., 2002). Therefore, it is impossible to establish an acoustic observation model as precise as GNSS (Fujita et al., 2006; Yamada et al., 2002; Yang et al., 2020).

It is well known that the ocean sound speed is the key parameter affecting the underwater acoustic positioning and navigation (Sato and Fujita, 2004). A commonly used method is to employ the sound speed profile (SSP) measurements to correct the ray refraction. As we could not get the SSP measurements point by point, the spatio-

Foundation item: The National Natural Science Foundation of China under contract No. 41931076; the National Center for Basic Sciences Project under contract No. 42388102; the Laoshan Laboratory under contract No. LSKJ202205100.
*Corresponding author, E-mail: zsq19981017@126.com

temporal interpolation methods have been employed to obtain the approximate sound speed parameter, such as the method based on the experiential orthogonal functions (EOF). In addition, an inversion method for instantaneous SSP area difference (Sun et al., 2024) and the sound speed field (SSF) based on back propagation (BP) neural network were developed which take the ocean temperature, salinity and pressure observations into account (Wang et al., 2020). A sound speed field forecasting based on the least square support vector machine proposed by Wang et al. (2024) may be helpful to construct the sound speed observation model. A positioning model with regard to elevation angles and sound speed error corrections has also been proposed (Liu et al., 2020, 2021).

However, subject to the spatio-temporal variation complexity of the sound speed, the sound speed error in SSP can cause a difference between the actual travel time and the calculated reference one. Therefore, the time error compensation models need to be developed by attributing the sound speed error to the time error (Kido et al., 2008; Kinugasa et al., 2020; Watanabe et al., 2020). In order to reduce the influence of sound speed variation, a compensation model with a time dilation factor was developed, in which the sound propagation time is multiplied by a dilation factor (Kido et al., 2008; Watanabe et al., 2020). Note that the Doppler effect can also be attributed to the time error effects (Asada and Yabuki, 2001; Ikuta et al., 2008; Xu et al., 2005), i.e., the Doppler shift bias parameter should be compensated in the acoustic observation equation when it is not corrected sufficiently at the signal cross-correlation processing (Zhang et al., 2025).

In order to compensate the sound speed temporal perturbations, an additional error term can be added to the observational model by the local polynomial or B-spline model (Fujita et al., 2004, 2006; Zhang et al., 2023). If the error compensation of the sound speed variation is taken into account more finely, then the gradient effects of the sound speed relative to the reference speed should be added to the observational model (Kido, 2007; Kinugasa et al., 2020; Ming et al., 2023; Yasuda et al., 2017; Yokota et al., 2019). Meanwhile, the sound speed variation estimated from GNSS-A data may reflect some ocean structures (Yokota et al., 2019).

A so-called resilient acoustic observation model with constant speed error compensation term, time bias compensation term and periodic terms was proposed (Qin et al., 2022; Wang et al., 2023; Yang and Qin, 2021). These models accord with the best fitting degree of observation residuals by considering the physical mechanism more exactly, thus achieving better positioning accuracy. In addition, the separation of different parameters is addressed well through iterative refinement.

This paper focuses on the time bias model analysis and finer sound speed spatio-temporal structure. Firstly, Section 2 summarizes the existing two classic models compensating for sound speed error. Then a time split model is proposed in Section 3, in which the sonar propagation time is presented by the sum of the theoretical time and a bias. Meanwhile, the physical meanings of the proposed model are analyzed. In Section 4, an optimal single-layer model and multi-layer model are developed, based on the sound speed perturbation model with two-layer spatial gradients, to improve the positioning accuracy by constructing a more reasonable sound speed structure. Section 5 verifies the effectiveness of the proposed models by using Japanese open data. Finally, conclusions are given in Section 6.

2 Time ratio model compensating for sound speed error

GNSS-A positioning generally adopts the round-trip time observations. The sea-surface transducer transmits an acoustic ranging signal to the seafloor transponder, then the transponder retransmits the signal to the sea-surface transducer, finally the sea-surface transducer receives the retransmitting signal. The signal round-trip travel time is denoted as t_{ij}. Let $\bar{t}_{ij}$ be the theoretical value of the signal round-trip traveling interval. Subject to complexity of the ocean environment, it is inevitable that the signal travel time period t_{ij} does not equal to the theoretical time period $\bar{t}_{ij}$, i.e., $t_{ij} \neq \bar{t}_{ij}$. In order to improve the seafloor acoustic positioning accuracy, firstly, the accuracy of acoustic range measurement should be improved. If the ranging error is attributed to the acoustic signal propagation time error, then the range error influence can be expressed by time error compensation term. To represent the sound speed variation, the time radio model was first proposed by Kido (Kido et al., 2008), while the early version of Nadir Total Delay (NTD) model (Honsho and Kido, 2017; Tomita et al., 2019; Xue et al., 2023) was presented as well.

$$a = \frac{t_{ij}}{\bar{t}_{ij}}, \tag{1}$$

$$\delta t = \left(t_{ij} - \bar{t}_{ij}\right)\cos\theta, \tag{2}$$

where, the ratio a and the normalization of time residual δt both represent sound speed variation; θ denotes the slant angle. The two models have played an important role for GNSS-A positioning in the following decade. Chen (2014) proved that the two models are equivalent when applying a moving survey.

Furthermore, when $a = 1$ in Eq. (1), the theoretical time is the same as the observation time, meaning that there is no systematic error in the acoustic propagation. If the perturbation λ of the acoustic signal traveling time is introduced, we need to find a particular function $a = f(\lambda)$ such that it is monotonic around 0 and $f(0) = 1$. Watanabe et al. (2020) adopted $a = e^{\lambda}$, that is, the acoustic signal traveling time is expressed as

$$t_{ij} = \mathrm{e}^{\lambda}\bar{t}_{ij} + \Delta_{ij}, \tag{3}$$

where Δ_{ij} denotes the random error. To separate the discrepancy ratio from the theoretical time $\bar{t}_{ij}$, a logarithmic transformation to the observation model (3) was proposed (Watanabe et al., 2020), and it reads

$$\ln(t_{ij}) = \ln(\bar{t}_{ij}) + \lambda + \Delta'_{ij}, \tag{4}$$

where $\ln(t_{ij})$ is the virtual observation, Δ'_{ij} is the random error of the virtual observation, λ is a systematic error term.

However, from Eq. (3) to Eq. (4), the distribution of the random error vector Δ'_{ij} is not clear for us. Furthermore, the relation of Δ'_{ij} and Δ_{ij} is following:

$$\Delta'_{ij} = -\ln\left(1 - \frac{\Delta_{ij}}{t_{ij}}\right). \tag{5}$$

From the relation of Δ'_{ij} and Δ_{ij}, we find that the extra error caused by the nonlinear time conversion in Eq. (4) can be ignored only when the relative observation accuracy is high enough.

3 Time split model compensating for the acoustic ranging error

In order to avoid the logarithmic operation in Eq. (4), we chose the function $a = \lambda + 1$ to construct GNSS-A positioning equation, which also satisfies monotone around 0 and equals 1 at 0. Then we have:

$$t_{ij} = (\lambda + 1)\bar{t}_{ij} + \Delta_{ij}. \tag{6}$$

Assume that there is a time bias δt_{ij} caused by the imperfection of the acoustic signal propagation, which results in

$$t_{ij} = \bar{t}_{ij} + \lambda\bar{t}_{ij} + \Delta_{ij} = \bar{t}_{ij} + \delta t_{ij} + \Delta_{ij}, \tag{7}$$

where δt_{ij} is the time bias in the acoustic signal traveling period, Δ_{ij} is the random error. The time error model expressed by Eq. (6) is called as discrepancy split model or split model for short.

The bias δt_{ij} is multi-sourced, such as the hardware delay of the seafloor transponder and the time bias due to the doppler effect. Comparing the two kinds of time error models expressed by Eq. (3) and Eq. (6), we find the following facts.

1) The time split model does not change the original time error distribution, which results in simpler calculation and easier error analysis. It is obvious that the time split model (6) avoids the nonlinear transformation, therefore, we recommend the model (6) as a basis to establish the acoustic observation model.

2) The time split model (6) closely connects to the time ratio model (3), we have approximately $\mathrm{e}^{\lambda} = 1 + \lambda$ at $\lambda = 0$. Therefore, the model (6) is nearly the same as the time ratio model (3), but the related acoustic range error model is easier to be established based on the time split model (6). It should be noted that the ratio model and the time split model have a similar performance of high-accuracy.

3) The time split model can be easily proved to be equivalent to the NTD model.

$$\bar{t}_{ij} = \int \frac{1}{C(u)\cos\theta}\mathrm{d}u \approx \frac{1}{\cos\theta}\int \frac{1}{C(u)}\mathrm{d}u = \frac{1}{\cos\theta}\cdot T^{*}, \tag{8}$$

where θ is the slant angle of the ray, T^{*} is the reference time of the signal traveling time along the vertical direction, $C(u)$ is the measured sound speed profile using a conductivity-temperature-depth (CTD) or an expendable bathy-thermograph (XBT) profiler. Then Eq. (6) can be transformed into:

$$t_{ij} = \bar{t}_{ij} + \lambda\bar{t}_{ij} + \Delta_{ij} \approx \bar{t}_{ij} + \frac{1}{\cos\theta}\lambda T^{*} + \Delta_{ij}. \tag{9}$$

It can be found that Eq. (9) and Eq. (2) have similar expressions through transformation, so they should have similar performance when taking a moving survey.

4) The physical meanings of the time split model are diverse. There are, at present, mainly three factors leading to the time error, namely the hardware delay, Doppler effect and sound speed variation. If only the hardware time delay is considered, $\delta t_{ij} = \Delta t_j$, where Δt_j is the hardware time delay of jth transponder. If only the Doppler effect is considered, then $\delta t_{ij} = \frac{1}{c}\frac{d\rho}{dt}\Delta t$, where ρ is the Euclidean distance between the transponder and the transducer, c is the sound speed. Meanwhile, as we mentioned earlier, if only sound speed variation is considered, $\delta t_{ij} = \lambda\bar{t}_{ij}$, where λ represent sound speed variation.

4 Sound speed perturbation model with optimal single-layer gradient and multi-layer gradients

Considering the importance of sound speed error in underwater positioning, we only discuss the sound speed perturbation based on Eq. (6) in this section. As mentioned above, whichever model is chosen, the key is how to model the distribution λ. A reasonable assumption is that the sound speed structure is stable within a short time, so local polynomials and B-splines are widely used in previous studies. For example, the smooth spline additive model in (Watanabe et al., 2020):

$$\lambda = a_0(T) + \frac{P}{L^{*}}a_1(T) + \frac{X}{L^{*}}a_2(T), \tag{10}$$

where $a_0(T)$, $a_1(T)$ and $a_2(T)$ are the cubic B-Spline models, $a_0(T)$ represents the temporal variation of sound

speed, $a_1(T)$ and $a_2(T)$ denote the temporal variations of horizontal gradients in deep and shallow seawater, respectively. X is the coordinate difference vector between the sea-surface transducer position and the centric position of the surface tracking trajectory, P is the coordinate difference vector between the seafloor transponder position and the centric position of the seafloor geodetic array, L^* is the reference distance between the transducer and transponder. The smooth additive spline model has interpretability, and it makes good use of the local features of GNSS-A observations, thus achieving better positioning results.

The positioning performance of the spline model depends a good deal on the construction of smoothness constraints (may also be known as the prior stochastic model of parameters), which needs additional estimation criterion. Our goal, in this paper, is to see how we can build a function model more reasonably under the same hyperparameter settings in order to improve positioning accuracy, and this is related to the spatio-temporal structure of sound speed.

As shown in Fig. 1, the transducer and seafloor transponders are placed in the local-coordinate system. Red line represents the vertical profile at the coordinate system's origin, and we assume that its sound speed structure is the same as the reference sound speed profile. The single-layer spatial gradient model different from Eq. (10) which considers gradients in shallow and deep layers, is arrived on the assumption that there is the spatial variation of sound speed within only one certain layer. To simplify the model, it is assumed that acoustic rays propagate along straight lines. The height difference between the transducer and the transponder is H, and there is a horizontal gradient caused by marine physical processes at depth h_l, satisfying $\frac{h_l}{H} = f_l \in (0, 1)$. Meanwhile, the horizontal coordinate vector of the point on acoustic ray at depth h_l is S_l. At this point, the sound speed perturbation model with a single-layer spatial gradient can be expressed as:

$$\lambda = a_0(T) + \frac{S_l}{L^*} a_l(T), \tag{11}$$

where, $a_l(T)$ is the cubic B-spline model, denoting the change of horizontal gradient corresponding to S_l at depth

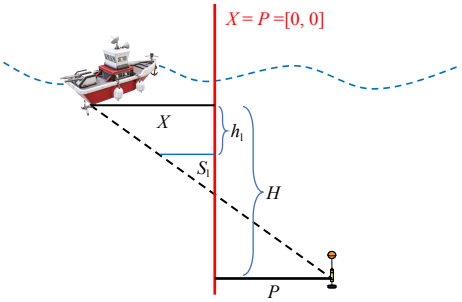

Fig. 1. Single-layer spatial gradient model.

h_l. The following equation can be given according to the geometric relationship shown in Fig. 1:

$$\frac{S_l - X}{P - X} \approx \frac{h_l}{H} = f_l, \tag{12}$$

where, X and P denote the positions of transducer and transponder in the local coordinate system, respectively. And by deduction, we have:

$$S_l = f_l P + (1 - f_l) X. \tag{13}$$

It can be seen that S_l is a function of X and P. Putting it into Eq. (11) and we have:

$$\lambda = a_0(T) + \frac{f_l P}{L^*} a_l(T) + \frac{(1 - f_l) X}{L^*} a_l(T). \tag{14}$$

Simultaneously considering Eqs (10) and (14) we further obtain that:

$$f_l = \frac{a_1}{a_1 + a_2}. \tag{15}$$

This indicates that two-layer model in Eq. (10) is related to single-layer model expressed in Eq. (14). From the expressions above, we find that the depth of single layer can be derived from the estimated two-layer spatial gradient variation based on Eq. (15) on one hand and on the other hand, the single-layer gradient variation can be decomposed into deep and shallow layers.

When the single-layer model is adopted, the key issue is to determine the depth of water layer, i.e., f_l. We propose a strategy for selecting optimal single-layer depth, that is, we can decompose the depth into a series of single layer depth f with equal intervals in (0, 1), based on the assumption that the roughness of the spline curve is fixed, and then the optimal depth is determined based on the criterion that the positioning residual is minimum. The number of parameters and the prior stochastic model do not change during the whole process, while only the depth of single layer changes.

As shown in Fig. 2, when the complex sound speed structure exists in the ocean, the sound speed perturbation containing multi-layer spatial gradients can be derived based on single-layer model (This assumes that there are n layers):

$$\lambda = a_0(T) + \sum_{i=1}^{n} \frac{S_i}{L^*} a_i(T). \tag{16}$$

By substituting the Eq. (13) in Eq. (16), we can get:

$$\lambda = a_0(T) + \sum_{i=1}^{n} \frac{f_i P}{L^*} a_i(T) + \sum_{i=1}^{n} \frac{(1 - f_i) X}{L^*} a_i(T), \tag{17}$$

where, f_i represents scaling factor corresponding to ith layer; $a_i(T)$ is the cubic B-spline model describing spatial

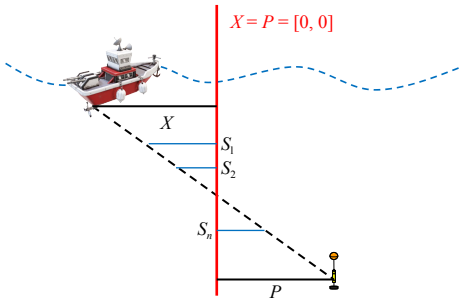

Fig. 2. Multi-layer spatial gradient model.

gradient variation at *i*th layer. When assuming that the roughness of spline models in all layers is the same, Eq. (17) can be transformed into:

$$\lambda = a_0(T) + \left(\sum_{i=1}^{n} \frac{f_i P}{L^*}\right) a_l(T) + \left(\sum_{i=1}^{n} \frac{(1-f_i)X}{L^*}\right) a_l(T). \quad (18)$$

This greatly reduces the complexity of the model while keeping the same number of parameters as Eq. (10) and makes sound speed perturbation model more flexible.

Similar to the single-layer model, what matters is how to choose proper layers where spatial gradients need to be considered. Based on the strategy adopted by single-layer model, the residual standard deviations of all layers are sorted from the minimum to the maximum, and the first few layers are used for building multi-layer horizontal gradient positioning model. During the whole of this session, the complexity of the multi-layer model is the same as Eq. (10), but thinking of more delicate structure of sound speed disturbance.

5 Calculation and analysis

5.1 *Data introduction*

Japanese opened data are used to perform the calculation and analysis (Watanabe et al., 2021). MYGI site is used to evaluate the positioning performance due to the complex sound speed structure in the northeast area of the Japan Trench, where the well-known Kuroshio Current shows a meandering path (Liu et al., 2023). GNSS-A data collected by MYGI station in April 2012 is used to verify the proposed time split model. As shown in Fig. 3, there are 8 seafloor geodetic stations in MYGI seafloor geodetic array, and 41.3 hours observations were obtained from April 22 to April 24, 2012. Meanwhile, the experimental observations used in the test computation contain 8-repeated sessions (S01–S08) which provides a convenience for performing the positioning accuracy verification and comparison. Every session had the same trajectory on the sea surface, as shown by the blue lines in Fig. 4.

To validate the proposed single-layer and multi-layer sound speed perturbation models, 28 sessions of MYGI station from December 2012 to June 2020 are used to calculate long-term displacements of seafloor array. We analyze the coordinate time series in two modes, namely, the non-rigid array solution (Xue et al., 2024) and the rigid array solution (Watanabe et al., 2020). Compared with the former, the rigid array solution takes the geometry relationship between the transponders into account, thus smoother time series can generally be obtained.

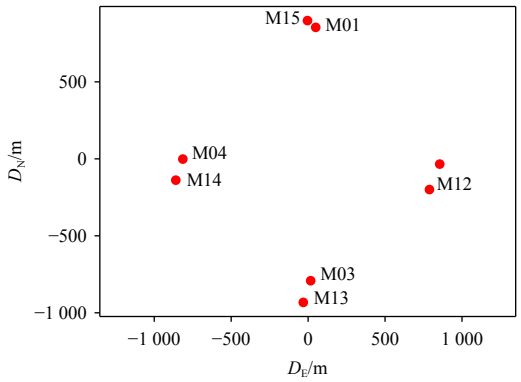

Fig. 3. MYGI seafloor geodetic network.

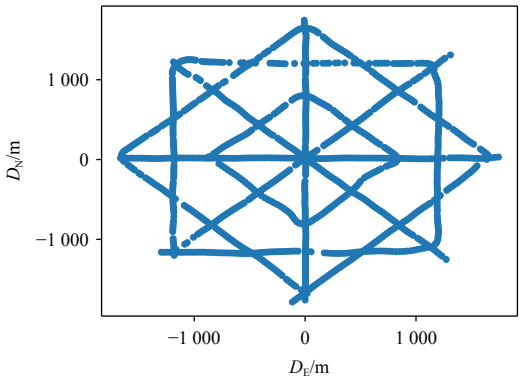

Fig. 4. Distribution of the sea-surface tracking lines (8 repeated tracks). D represents distance. E: east; N: north.

5.2 *Comparison of time split model with time ratio model*

Firstly, we employ the same parametrization strategy to solve the time split model (6) and time ratio model (3) adopted by GNSS-Acoustic Ranging combined Positioning Solver (GARPOS V1.0), i.e., adopting the same B-spline basis functions with the same smoothing parameters. The results calculated by model (6) are compared with the single-epoch solutions produced from GARPOS, shown in Table 1. The GARPOS software adopts the recommended default parameter settings.

It shows from Table 1 that the biggest coordinate difference between the two models does not exceed 4 cm. This means that the two models can be considered to be equivalent to each other for achieving centimeter-level accuracy positioning.

Figure 5 gives the residuals of the above two models. It shows that the standard deviation of residuals for both Model (6) and Model (3) is approximately 0.14 m and there is no significant difference. The high-precision ob-

Table 1. Comparison of the proposed time split model with GARPOS model

Station	Time split model			GARPOS			Differences		
	D_E	D_N	D_U	D_E	D_N	D_U	ΔD_E	ΔD_N	ΔD_U
M01	49.170	854.176	−1 659.442	49.143	854.177	−1 659.444	0.027	0.001	0.002
M03	16.328	−791.520	−1 673.867	16.297	−791.536	−1 673.871	0.031	0.017	0.005
M04	−814.431	−1.348	−1 666.917	−814.464	−1.358	−1 666.897	0.033	0.010	0.020
M05	854.900	−33.930	−1 677.945	854.891	−33.933	−1 677.967	0.009	0.003	0.022
M12	788.295	−199.421	−1 676.583	788.276	−199.426	−1 676.607	0.019	0.005	0.023
M13	−31.421	−932.524	−1 675.471	−31.454	−932.532	−1 675.476	0.032	0.008	0.005
M14	−859.953	−138.444	−1 668.304	−859.978	−138.450	−1 668.285	0.025	0.006	0.019
M15	−4.248	898.134	−1 659.589	−4.274	898.126	−1 659.593	0.026	0.008	0.004
Center	−0.170	−43.110	−1 669.765	−0.195	−43.117	−1 669.767	0.025	0.007	0.002

servations make additive error compensation model approximately equivalent to multiplicative error compensation model.

Figure 6 shows positioning results from these two models based on the 8-repeated session observations. A reasonable assumption is that the seafloor station remains stable within two days, so the standard deviation of the positioning series is important in the evaluation of model. The standard deviations of coordinate series corresponding to GARPOS are 0.043 m, 0.029 m and 0.090 m, for the north, east and up components, respectively. The standard deviations of coordinate series corresponding to the time split model are 0.044 m, 0.026 m and 0.087 m, for the north, east and up components, respectively. It can be found that the time split model proposed in this paper can provide the positioning results as accurate as those produced from the opened GARPOS V1.0. It should be highlighted that the strategy for selecting hyperparameters in the model might be optimized to further improve the positioning accuracy.

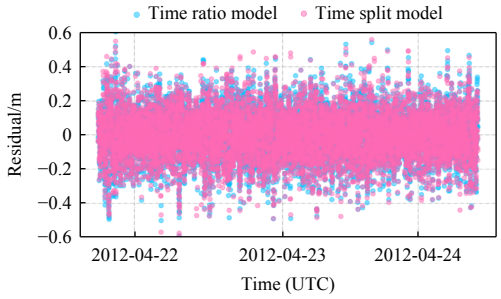

Fig. 5. Residual of time split model and GARPOS model.

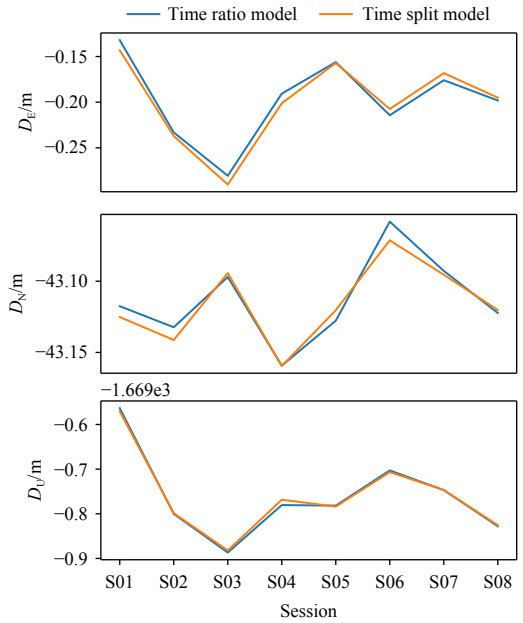

Fig. 6. Positioning series of 8 repeated test segments of the center point of the network in Fig.3. U: up.

5.3 *Comparison of different sound speed perturbation model under non-rigid array*

To compare the positioning performance of different sound speed perturbation models, three schemes are adopted to obtain long-term coordinate series with non-rigid array. It should be noted that all sound speed perturbation models are based on the proposed time split model. In order to evaluate the positioning accuracy of different schemes, linear model $X(t) = Vt + X_0 + \Delta$ is used to fit the time series of coordinate, where X denotes the three-dimensional coordinate vector of the seafloor array center; V denotes the estimated displacement velocity vector of the seafloor array center; Δ denotes the random error vector. The residual standard deviation (STD) of linear fitting can reflect the positioning performance under different schemes.

Scheme 1: two-layer spatial gradient model (including shallow and deep layers) is adopted to estimate the coordinates of transponders, and the Akaike's Bayesian Information Criterion (ABIC) criteria is used to obtain optimal smoothness of B-spline functions (Watanabe et al., 2020). Specifically, let $\mu_0/\mu_i = 10$, where μ_0 is the smoothness parameter for $a_0(T)$, and μ_1 is the smoothness parameter for the horizontal gradient. Then the method for searching the parameter μ_0 is adopted to perform smoothness searching by minimizing ABIC.

Scheme 2: with the same hyperparameters as in Scheme 1, the single-layer spatial gradient model is employed.

Scheme 3: with the same hyperparameters as in Scheme 1, the multi-layer spatial gradient model is adopted.

Figure 7 shows the first three optimal layers selected by positioning residual STD (the resolution of f is 0.1), with blue, orange and green dots standing for first, second and third layer respectively. Scheme 2 only adopts the first layer, and Scheme 3 adopts three layers. It can be seen from Fig. 7 that the optimal depth for horizontal gradient is less than 0.4 h for most of the time. It indicates that the spatial variation of sound speed usually happens in the shallower layer and the sound speed structure near seafloor is stable.

Figure 8 shows the positioning results of three schemes under the non-rigid solutions. The black hollow circles represent the time coordinate series of Scheme 1, and the black lines illustrate the corresponding linear trend of array displacements. The blue triangle symbols represent the time coordinate series of Scheme 2, and the blue lines show the corresponding linear trend of array displacements. The red triangle symbols represent the coordinate time series of Scheme 3, and the red lines show the corresponding linear trend of array displacements. The station velocity and residual STD of different schemes are presented in Table 2.

According to Table 2, the differences of E/N/U station velocities between Scheme 1 and Scheme 2 are 0.10 cm/a, 0.29 cm/a and 0.02 cm/a, respectively. The modification in the sound speed perturbation model has an impact on the estimation of station velocity. The residual STD corresponding to Scheme 1 are 3.86 cm, 5.19 cm and 8.28 cm for the east, north and up components, respectively, while those of Scheme 2 are 3.95 cm, 4.60 cm and 8.23 cm for the east, north and up components. The overall positioning performance of Scheme 2 is superior than that of Scheme 1, especially in the N and U directions, demonstrating that the optimal single-layer gradient model is conducive to improving positioning accuracy. However, the residual STD of Scheme 2 is worse than that of Scheme 1 in the E direction, which suggests that there may be more complex sound speed structure and multi-layer sound speed gradient model should be considered.

It can be seen from Table 2 that the station velocity of Scheme 1 is similar to that of Scheme 3. The differences of E/N/U station velocities between the two schemes are 0.02 cm/a, 0.05 cm/a and 0.04 cm/a, respectively. Meanwhile, the residual STD corresponding to Scheme 1 are 3.86 cm, 5.19 cm and 8.28 cm for the east, north and up components, respectively, while those of Scheme 3 are 3.54 cm, 4.79 cm and 8.09 cm for the east, north and up components, with the improvement of 8.3%, 7.7% and 2.3%. In a word, Scheme 3 has better positioning accuracy while keeping the same estimation of station velocity as Scheme 1, indicating that the proposed multi-layer sound speed perturbation model weakens the influence of complex sound speed structure, to some extent. It should be emphasized that the number of parameters and prior stochastic models of different models are the same, which means that the sound speed model does not become more complex although more fine structures are considered.

5.4 *Comparison of different sound speed perturbation under rigid array*

Similar to the ways under non-rigid array, three

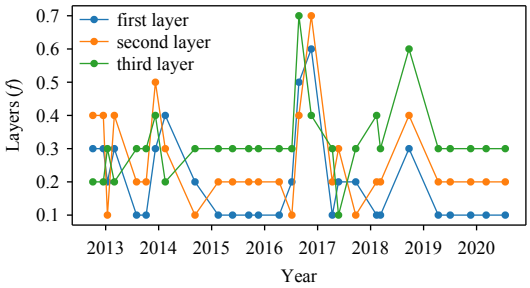

Fig. 7. Selected optimal layers.

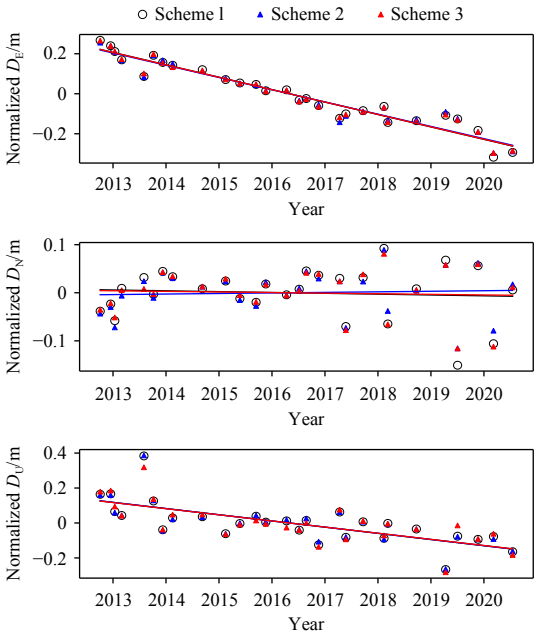

Fig. 8. Solutions of three schemes.

Table 2. Displacement time series analysis of three schemes

Scheme	Station velocity			Residual STD		
	V_E/(cm·a^{-1})	V_N/(cm·a^{-1})	V_U/(cm·a^{-1})	R_E/cm	R_N/cm	R_U/cm
Scheme 1	−6.21	−0.17	−3.55	3.86	5.19	8.28
Scheme 2	−6.11	0.12	−3.53	3.95	4.60	8.23
Scheme 3	−6.19	−0.12	−3.51	3.54	4.79	8.09

Note: V represents velocity; R, normalized distance STD.

schemes are employed to obtain the long-term time series of coordinate with rigid array. The linear model is also adopted to obtain linear trend of positioning results. It should be noted that the geometry relationship between transponders is determined using the time series of Scheme 1 with non-rigid array in Section 5.3.

Scheme 1: based on rigid array, two-layer spatial gradient model (including shallow and deep layers) is adopted to estimate the coordinates of transponders.

Scheme 2: with the same hyperparameters as those in Scheme 1, the single-layer spatial gradient model is employed based on rigid array.

Scheme 3: with the same hyperparameters as those in Scheme 1, the multi-layer spatial gradient model is adopted based on rigid array.

The time coordinate series of the rigid array solution of three schemes are shown in Fig. 9, where the black hollow circles represent the coordinate time series of Scheme 1, and the black lines illustrate the corresponding linear trend of array displacements. The blue triangle symbols represent the coordinate time series of Scheme 2, and the blue lines show the corresponding linear trend of array displacements. The red triangle symbols represent the coordinate time series of Scheme 3, and the red lines show the corresponding linear trend of array displacements. The station velocities and residual STDs of different schemes are presented in Table 3.

It can be seen from Table 3 that the differences of E/N/U station velocities between Scheme 1 and Scheme 2 are 0.13 cm/a, 0.13 cm/a and 0.10 cm/a respectively, all of which are greater than 10 mm/a. The residual STDs of Scheme 1 are 2.92 cm, 3.31 cm and 3.56 cm for E, N and U directions respectively, while those of Scheme 2 are 3.06 cm, 3.16 cm and 3.42 cm for E, N and U directions

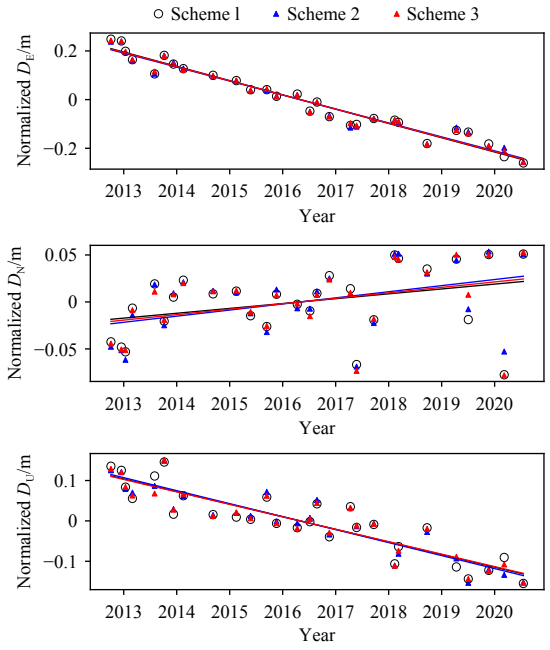

Fig. 9. Solutions of three schemes.

Table 3. Displacement time series analysis of three schemes

Scheme	Station velocity			Residual STD		
	V_E/ (cm·a^{-1})	V_N/ (cm·a^{-1})	V_U/ (cm·a^{-1})	R_E/cm	R_N/cm	R_U/cm
Scheme 1	−5.87	0.52	−3.12	2.92	3.31	3.56
Scheme 2	−5.74	0.65	−3.22	3.06	3.16	3.42
Scheme 3	−5.81	0.58	−3.08	2.80	3.27	3.42

respectively. It can be found that the rigid array solutions clearly outperform the non-rigid array solutions given in Section 5.3, and its positioning performances of different components are similar. Meanwhile, single-layer model has the improvement of 0.15 cm and 0.14 cm for the north and up components, indicating that the selection of optimal depth of gradient can improve positioning accuracy, only the residual STD in E direction of Scheme 2 is a little bit worse than that of Scheme 1.

According to Table 3, the differences of E/N/U station velocities between Scheme 1 and Scheme 3 are 0.06 cm/a, 0.06 cm/a and 0.04 cm/a respectively, all of which are less than 1mm/a. The residual STDs of Scheme 1 are 2.92 cm, 3.31 cm and 3.56 cm for E, N and U directions, respectively, while those of Scheme 3 are 2.80 cm, 3.27 cm and 3.42 cm for E, N and U directions. The multi-layer sound speed perturbation model has the improvement of 0.12 cm, 0.04 cm and 0.14 cm for E/N/U components, respectively, which means that the proposed model not only represents more reasonable sound speed structure, but also improves underwater positioning accuracy.

In both non-rigid solutions and rigid solutions, the proposed optimal single-layer gradient model and multi-layer gradient model could potentially improve underwater positioning accuracy. At the same time, they also provide flexibility to the construction of sound speed perturbation while maintaining the same model complexity. Therefore, based on above proposed models, there is no need to extract some ocean structures by using Eq. (15).

6 Conclusions

The underwater acoustic positioning errors come from complex ocean environment effects and the equipment hardware errors, as well as the model errors. Over the past two decades, scholars have suggested various acoustic positioning models from different viewpoints. Through formula derivation, it is shown that partial parameterization models might be approximately equivalent in a certain extend. It is recommended that the model has a concise form and specific physical meanings should be adopted.

For sound speed perturbation, the optimal single-layer gradient model and multi-layer gradient model are proposed based on the time split model. Under the non-rigid array, our results show that the scheme with the multi-layer sound speed perturbation model improves the position-

ing accuracy by about 8.3%, 7.7% and 2.3% for the east, north and up components. Meanwhile, for rigid array, the multi-layer sound speed perturbation model has the improvement of 0.12 cm, 0.04 cm and 0.14 cm for *E*/*N*/*U* components, respectively. This shows that the multi-layer sound speed perturbation model can improve positioning accuracy without an increase in model complexity. What's more, this does favor on understanding sound speed structure generated by ocean currents.

In summary, the time split model proposed in this paper should be recommended because this model compensates the time error in a direct linear manner without the nonlinear logarithmic transformation which increases the complexity of the error distribution. Moreover, more flexible sound speed perturbation models are beneficial to reduce the influence of sound speed variation, thus improving underwater positioning accuracy.

Acknowledgements

We are very grateful to Hydrographic and Oceanographic Department, Japan Coast Guard providing open seafloor geodetic data for this paper.

References

Asada A, Yabuki T. 2001. Centimeter-level positioning on the seafloor. Proceedings of the Japan Academy, Series B, 77(1): 7–12, doi: 10.2183/pjab.77.7

Chen Hsin-Hung. 2014. Travel-time approximation of acoustic ranging in GPS/Acoustic seafloor geodesy. Ocean Engineering, 84: 133–144, doi: 10.1016/j.oceaneng.2014.04.015

Chen Guanxu, Liu Yang, Liu Yanxiong, et al. 2019. Adjustment of transceiver lever arm offset and sound speed bias for GNSS-acoustic positioning. Remote Sensing, 11(13): 1606, doi: 10.3390/rs11131606

Fujita M, Ishikawa T, Mochizuki M, et al. 2006. GPS/Acoustic seafloor geodetic observation: method of data analysis and its application. Earth, Planets and Space, 58(3): 265–275, doi: 10.1186/BF03351923

Fujita M, Sato M, Yabuki T. 2004. Development of seafloor positioning software using inverse method. Technical Bulletin on Hydrography and Oceanography, (22): 50–56

Honsho C, Kido M. 2017. Comprehensive analysis of travel-time data collected through GPS-acoustic observation of seafloor crustal movements. Journal of Geophysical Research: Solid Earth, 122(10): 8583–8599, doi: 10.1002/2017JB014733

Ikuta R, Tadokoro K, Ando M, et al. 2008. A new GPS-acoustic method for measuring ocean floor crustal deformation: application to the Nankai Trough. Journal of Geophysical Research: Solid Earth, 113(B2): B02401, doi: 10.1029/2006JB004875

Kido M. 2007. Detecting horizontal gradient of sound speed in ocean. Earth, Planets and Space, 59(8): e33–e36, doi: 10.1186/BF03352027

Kido M, Osada Y, Fujimoto H. 2008. Temporal variation of sound speed in ocean: a comparison between GPS/acoustic and *in situ* measurements. Earth, Planets and Space, 60(3): 229–234, doi: 10.1186/BF03352785

Kinugasa N, Tadokoro K, Kato T, et al. 2020. Estimation of temporal and spatial variation of sound speed in ocean from GNSS-A measurements for observation using moored buoy. Progress in Earth and Planetary Science, 7(1): 21, doi: 10.1186/s40645-020-00331-5

Li Xingxing, Huang Jiaxin, Li Xin, et al. 2022. Review of PPP–RTK: achievements, challenges, and opportunities. Satellite Navigation, 3(1): 28, doi: 10.1186/s43020-022-00089-9

Liu Yang, Li Menghao, Liu Yanxiong, et al. 2023. Sequential GNSS-Acoustic seafloor point positioning with modeling of sound speed variation. Journal of Geodesy, 97(12): 115, doi: 10.1007/s00190-023-01810-5

Liu Yixu, Lu Xiushan, Xue Shuqiang, et al. 2021. A new underwater positioning model based on average sound speed. The Journal of Navigation, 74(5): 1009–1025, doi: 10.1017/S0373463321000400

Liu Yixu, Xue Shuqiang, Qu Guoqing, et al. 2020. Influence of the ray elevation angle on seafloor positioning precision in the context of acoustic ray tracing algorithm. Applied Ocean Research, 105: 102403, doi: 10.1016/j.apor.2020.102403

Ming Feng, Yang Yuanxi, Zeng Anmin. 2023. Positioning accuracy of GNSS-A in deep sea based on Bayesian estimation. Chinese Journal of Geophysics (in Chinese), 66(3): 951–960, doi: 10.6038/cjg2022P0791

Qin Xianping, Yang Yuanxi, Sun Bijiao. 2022. The refined resilient model for underwater acoustic positioning. Ocean Engineering, 266: 112795, doi: 10.1016/j.oceaneng.2022.112795

Qin Xianping, Yang Yuanxi, Sun Bijiao. 2023. A robust method to estimate the coordinates of seafloor stations by direct-path ranging. Marine Geodesy, 46(1): 83–98, doi: 10.1080/01490419.2022.2113578

Sato M, Fujita M. 2004. Effects of sound velocity profiles in the seafloor geodetic observation. Technical Bulletin on Hydrography and Oceanography, (22): 42–49

Sun Wenzhou, Yang Yuanxi, Zeng Anmin. 2024. Inversion method for instantaneous SSP area difference. Marine Geodesy, 47(2): 173–181, doi: 10.1080/01490419.2023.2285360

Tomita F, Kido M, Honsho C, et al. 2019. Development of a kinematic GNSS-Acoustic positioning method based on a state-space model. Earth, Planets and Space, 71(1): 102, doi: 10.1186/s40623-019-1082-y

Wang Junting, Xu Tianhe, Huang Wei, et al. 2024. Underwater sound speed field forecasting based on the least square support vector machine. Journal of Marine Science and Engineering, 12(3): 480, doi: 10.3390/jmse12030480

Wang Junting, Xu Tianhe, Liu Yangfan, et al. 2023. Augmented underwater acoustic navigation with systematic error

modeling based on seafloor datum network. Marine Geodesy, 46(2): 129–148, doi: 10.1080/01490419.2022.2162646

Wang Junting, Xu Tianhe, Nie Wenfeng, et al. 2020. The construction of sound speed field based on back propagation neural network in the global ocean. Marine Geodesy, 43(6): 621–642, doi: 10.1080/01490419.2020.1815912

Watanabe S, Ishikawa T, Nakamura Y, et al. 2021. GNSS-A data obtained at the sites along the Japan Trench from March 2011 to June 2020 (1.0. 0)[Data set]. Zenodo

Watanabe S, Ishikawa T, Yokota Y, et al. 2020. GARPOS: analysis software for the GNSS-A seafloor positioning with simultaneous estimation of sound speed structure. Frontiers in Earth Science, 8: 597532, doi: 10.3389/feart.2020.597532

Xu Peiliang, Ando M, Tadokoro K. 2005. Precise, three-dimensional seafloor geodetic deformation measurements using difference techniques. Earth, Planets and Space, 57(9): 795–808, doi: 10.1186/BF03351859

Xue Shuqiang, Li Baojin, Xiao Zhen, et al. 2023. Centimeter-level-precision seafloor geodetic positioning model with self-structured empirical sound speed profile. Satellite Navigation, 4(1): 30, doi: 10.1186/s43020-023-00120-7

Xue Shuqiang, Yang Yuanxi, Yang Wenlong, et al. 2024. GNSS-A network solution with zenith acoustic delay estimation. Marine Geodesy, 47(3): 237–268, doi: 10.1080/01490419.2024.2307932

Yamada T, Ando M, Tadokoro K, et al. 2002. Error evaluation in acoustic positioning of a single transponder for seafloor crustal deformation measurements. Earth, Planets and Space, 54(9): 871–881, doi: 10.1186/BF03352435

Yang Yuanxi, Ding Qun, Gao Weiguang, et al. 2022. Principle and performance of BDSBAS and PPP-B2b of BDS-3. Satellite Navigation, 3(1): 5, doi: 10.1186/s43020-022-00066-2

Yang Yuanxi, Liu Yanxiong, Sun Dajun, et al. 2020. Seafloor geodetic network establishment and key technologies. Science China: Earth Sciences, 63(8): 1188–1198, doi: 10.1007/s11430-019-9602-3

Yang Yuanxi, Qin Xianping. 2021. Resilient observation models for seafloor geodetic positioning. Journal of Geodesy, 95(7): 79, doi: 10.1007/s00190-021-01531-7

Yasuda K, Tadokoro K, Taniguchi S, et al. 2017. Interplate locking condition derived from seafloor geodetic observation in the shallowest subduction segment at the Central Nankai Trough, Japan. Geophysical Research Letters, 44(8): 3572–3579, doi: 10.1002/2017GL072918

Yokota Y, Ishikawa T, Watanabe S. 2019. Gradient field of undersea sound speed structure extracted from the GNSS-A oceanography. Marine Geophysical Research, 40(4): 493–504, doi: 10.1007/s11001-018-9362-7

Zhang Wenhao, Wang Jinling. 2023. Integrity monitoring scheme for single-epoch GNSS PPP-RTK positioning. Satellite Navigation, 4(1): 10, doi: 10.1186/s43020-023-00099-1

Zhang Shengqiu, Yang Yuanxi, Xu Tianhe. 2023. Estimation of ocean sound velocity variation based on GNSS-A and its influence on positioning. Chinese Journal of Geophysics (in Chinese), 66(3): 961–972, doi: 10.6038/cjg2022Q0202

Zhang Shengqiu, Yang Yuanxi, Xu Tianhe, et al. 2025. Long-range LBL underwater acoustic navigation considering Earth curvature and Doppler effect. Measurement, 240: 115524, doi: 10.1016/j.measurement.2024.115524

Zhao Jianhu, Zhang Hongmei, Wu Meng. 2021. A sound ray tracking algorithm based on template-interpolation of constant-gradient sound velocity. Geomatics and Information Science of Wuhan University (in Chinese), 46(1): 71–78, doi: 10.13203/j.whugis20180405